JOURNAL OF MATERIALS SCIENCE **39** (2004) 1233– 1239

Dielectric and thermal properties of xPbTiO$_3$-(1 − x)SrTiO$_3$ Polycrystals

E. MARTÍNEZ
CICESE, Physics of Materials Graduate Program, Km. 107 Carr. Tijuana—Ensenada, C.P. 22800, BC. México

S. GARCÍA, E. MARIN, O. VASALLO
Facultad de Física-IMRE, Universidad de la Habana, Vedado, La Habana 10400, Cuba

G. PEÑA-RODRÍGUEZ, A. CALDERÓN
CICATA-IPN, Legaria 694, 11500 México D.F.

J. M. SIQUEIROS
Centro de Ciencias de la Materia Condensada, UNAM C.P. 2681, B.C., México
E-mail: jesus@ccmc.unam.mx

SrTiO$_3$ and PbTiO$_3$ perovskites are combined to form the xPbTiO$_3$-(1 − x)SrTiO$_3$ (PST) solid solution. In this work, a study of its dielectric and thermal properties is reported as a function of PbTiO$_3$ content. The dielectric properties of the xPbTiO$_3$-(1 − x)SrTiO$_3$ solid solution are determined through a thermoelectric analysis technique and hysteresis measurements. Such measurements made at room temperature for all compositions show the influence of one component upon the other resulting in a response to the electric field that involves a strained lattice behavior. A limiting case of antiferroelectric-like behavior is observed for $x = 0.5$. The thermal properties such as the specific heat capacity (c) and thermal diffusivity (α) were determined using a photoacoustic technique (PA) and the temperature relaxation method (TRM). The thermal conductivity was calculated from the results obtained for c and α.

1. Introduction

Nowadays, there is considerable interest in crystalline and polycrystalline ferroelectric materials due to their many known and potential applications [1]. In the design of devices based in ferroelectrics, it is very important to take into account the thermal properties of the involved materials, because the rate at which the generated heat inside the device dissipates, may determine its performance and lifetime [2]. As an example, to enhance the operating parameters of integrated pyroelectric IR-sensors the thermal properties must be improved for the optimal functioning. A low thermal conductivity is essential for materials used as pyroelectric detectors [3]. It is well known that thermal properties of dielectric ceramics, especially the ferroelectric ones, are directly related to their microstructure where phonon propagation accounts for the transport of thermal energy. Therefore, the understanding of the correlation between microstructural aspects and thermal properties is of great importance [2]. That is, since the dielectric behavior is temperature dependent, their response to heat exchange phenomena will be of relevance, whether they are used as pyroelectric detectors, memory elements or high permittivity capacitors. Heat capacity and thermal conductivity are fundamental in fixing the resistance to thermal stresses and also determine operating temperatures and temperature gradients [2]. Solid solutions such as (Pb$_x$Sr$_{1-x}$)TiO$_3$ have received some attention when looking for a material with intermediate properties (dielectric properties) between those of the extreme compositions (PbTiO$_3$ and SrTiO$_3$) [4–6], however, the knowledge of the thermal properties for mixtures of PbTiO$_3$ and SrTiO$_3$ perovskites has not been reported before.

In this work we investigate the dielectric and thermal properties of a system that consist of a mixture of PbTiO$_3$ and SrTiO$_3$ perovskites that we call xPbTiO$_3$-(1 − x)SrTiO$_3$. Among the thermal properties studied are the specific heat capacity (c), the thermal diffusivity (α) and the thermal conductivity (k) for xPbTiO$_3$-(1 − x)SrTiO$_3$ ($x = 0.1, 0.3, 0.5, 0.7, 0.9$) ceramic samples using a photoacoustic (PA) technique [7, 8] and the temperature relaxation method (TRM) [9].

2. Experimental procedure

High purity (>99.9%) PbTiO$_3$ and SrTiO$_3$ powders were used for the preparation, via the conventional ceramic technique, of the nominal composition xPbTiO$_3$-(1 − x)SrTiO$_3$, where x is 0.1, 0.3, 0.5, 0.7 and 0.9. The powders were mixed in an agate mortar with ethyl alcohol for 2 h and heated at 1300°C for 2 h. The resulting powders were uniaxially die-pressed at

6 MPa into discs of 10-mm diameter and 1 mm thickness. Silver electric contacts were deposited onto the samples for electrical measurements. The temperature dependence of the dielectric constant ($\varepsilon/\varepsilon_o$) was measured using an LCR bridge (PHILIPS PM 6303) working at the fixed frequency of 1 kHz. A Radiant Technologies Precision Pro Analyzer with Vision Software was used to evaluate the electrical properties at high voltages. The thermal diffusivity measurements were carried out using the photoacoustic technique (PA) in a heat transmission configuration. The specific heat capacity measurements were obtained by the temperature relaxation method (TRM). The results of both techniques were combined to determine the thermal conductivity of the samples for each relative concentration.

3. Results and discussion

3.1. Dielectric analysis

The dielectric constant ($\varepsilon/\varepsilon_o$) was evaluated, as a function of temperature, at 1 kHz, for each composition of the xPbTiO$_3$-$(1-x)$SrTiO$_3$ polycrystalline samples. The samples were first heated to 500°C and measured in cooling until they reached room temperature to look for the paraelectric-ferroelectric transition as a function of composition. In Fig. 1 the dielectric constant behavior with temperature shows the phase transitions as functions of relative concentration. For $x = 0.1$ a relatively weak, but well defined transition appears at a temperature T_c very near that of pure PbTiO$_3$ (457°C). At such low concentration of the polar phase, it seems that a dominant SrTiO$_3$ phase remains in the paraelectric state and the polar behavior is entirely attributed to a lead titanate influenced phase. Similar behavior occurs for $x = 0.3$.

The influence of one phase upon the other becomes particularly evident for the intermediate concentrations around $x = 0.5$ where a highly stressed structure is formed forcing the cells into a reduced symmetry configuration which manifests as a polar behavior at temperatures far from those of the extreme concentrations. For $x = 0.5$ a broad but well defined phase transition appears at 67°C showing very high permittivity values [10] and a peculiar hysteretic behavior that will be discussed ahead in this paper. Once the material is formed with a specified composition, tetragonal and cubic cells will coexist in each crystallite in the corresponding ratio producing a new stressed structure with its own characteristic properties (Fig. 2a). Therefore a transition associated to the strained SrTiO$_3$, which in a pure state appears at very low temperatures, shifts to higher temperatures as the polar behavior is enhanced due to stress. Fig. 2b shows such behavior. For $x = 0.7$ two peaks are present in the considered temperature range, one at 189°C and the other at 352°C making evident the mutual influence between the two component phases. For $x = 0.9$ there is a transition at 334°C associated to the modified tetragonal phase PbTiO$_3$. As the pure PbTiO$_3$ phase is approached, the influence of the SrTiO$_3$ fades and the transition temperature approaches that of lead titanate. It is expected that the transition associated to SrTiO$_3$ also be present at very low temperatures as the influence of one phase upon the other becomes less important. These results are very different from those obtained by other authors [4–6] due to the coexistence of both phases in the extreme concentrations. This reason explains the non-linear behavior between transition temperature and composition. Even for $x = 0.5$ the transition temperature is not coincident with that reported for a stoichiometric system [6].

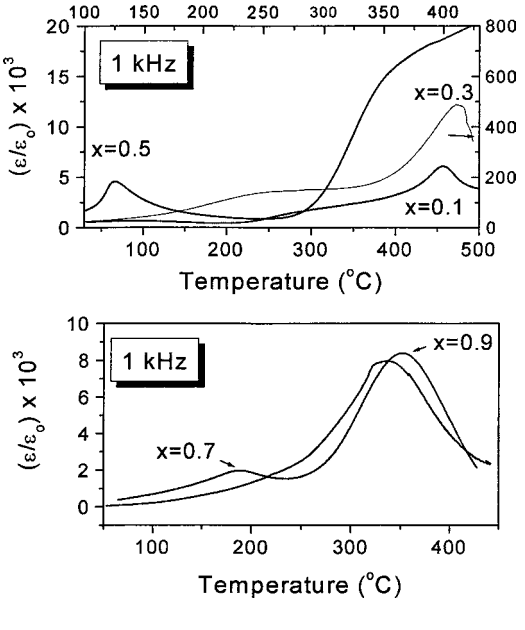

Figure 1 Dielectric constant as a function of temperature measured at 1 kHz.

3.2. Polarization features at room temperature

The P vs. V behavior corresponding to all compositions may be explained by the coexistence of two strongly interacting crystal phases. For $x = 0.1$ we have a minority tetragonal PbTiO$_3$ polar phase at high temperature exerting a weak influence on the non polar SrTiO$_3$ phase, leading to a slightly non-linear electrical response as shown in Fig. 3. The ferroelectric features of such a small quantity of PbTiO$_3$ are diluted in an essentially paraelectric matrix. Correspondingly, a dominating SrTiO$_3$ cubic phase is essentially observed in the crystallographic studies [10]. As the PbTiO$_3$ relative concentration is increased, a stronger interaction between the two phases is expected leading to a resulting strained structure. For $x = 0.3$ a measurable ferroelectric behavior from the hysteresis loop is observed, making evident the presence of a non-cubic phase. For $x = 0.5$, a peak in the ($\varepsilon/\varepsilon_o$) vs. temperature curve at 67°C indicates a phase transition associated to a strained structure resulting from a strong interaction between the two phases (Fig. 1). For this particular composition it is interesting to notice in Fig. 3 an antiferroelectric-like behavior in the P vs. V curves associated to such strained structure. This behavior can be understood in terms of the strongly stressed hybrid structure that leads to an antiparallel alignment

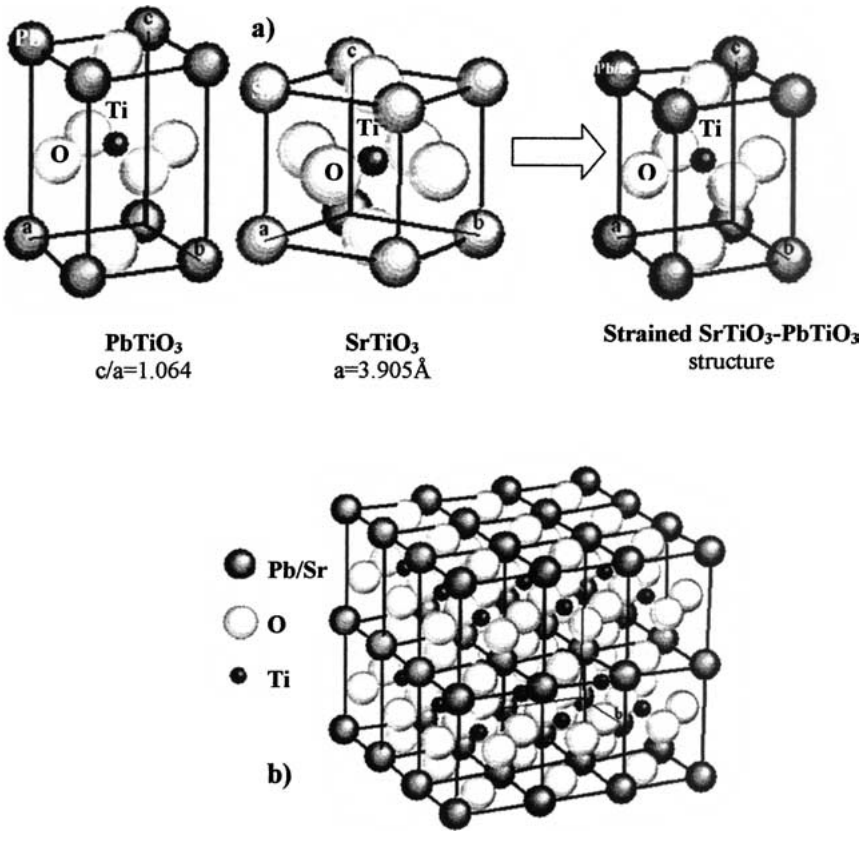

Figure 2 (a) Coexistence of $PbTiO_3$ and $SrTiO_3$ could origin a stressed structure as shown. (b) Scheme that represents a global stressed structure for $x = 0.5$.

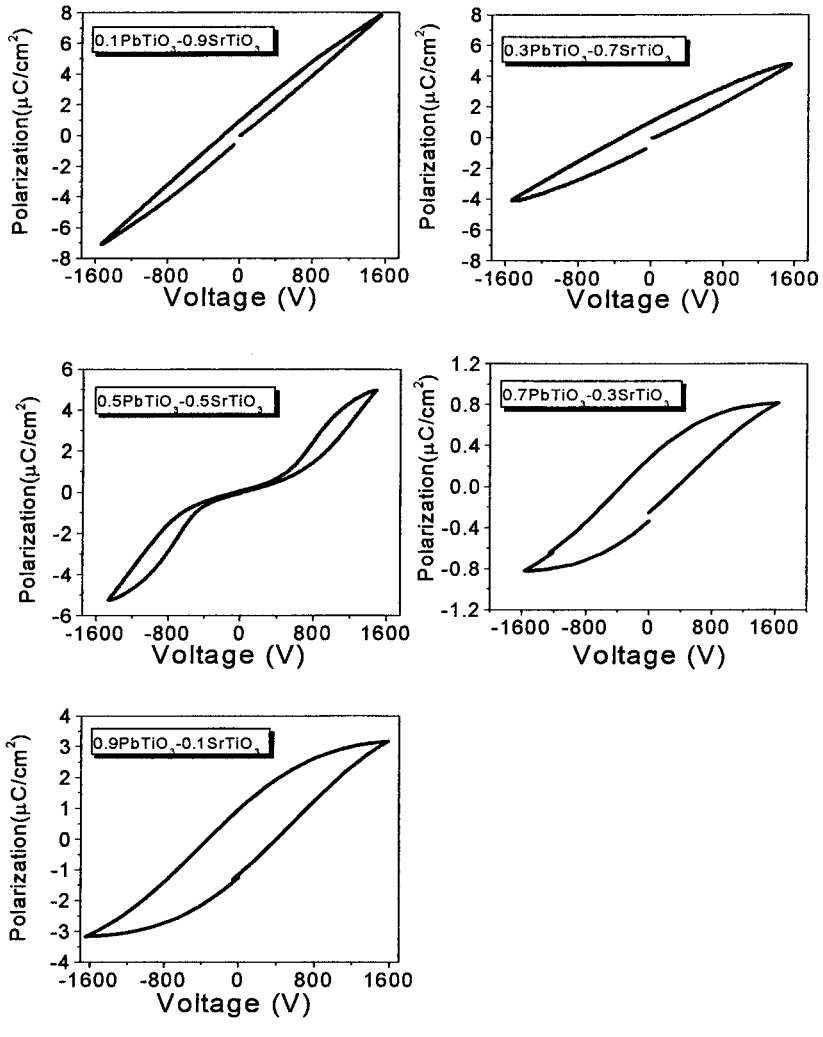

Figure 3 Polarization vs. voltage curves for the $x PbTiO_3$-$(1-x)SrTiO_3$ system.

of the 180° domains to achieve a minimum energy configuration. By applying an external electric field it is possible to orient ferroelectric domains in the direction of the field to produce polarization of the sample, however, this polarization disappears as the electric field is turned off. For $x = 0.7$ and 0.9, the response of the samples departs from the stressed-structure behavior and the contribution to polarization increases as would be expected due to its higher $PbTiO_3$ concentration showing slim well defined hysteresis loops with low values of the polarization. The sample is depicted as a polar matrix with paraelectric regions that interrupt long-range order. Even though the $PbTiO_3$ tetragonal phase is the more abundant, the coexistence with a non-polar phase strongly deteriorates its ferroelectric properties.

3.3. Thermal properties measurement

The thermal diffusivity (α) and the specific heat capacity (c) of the samples were measured using the photoacoustic (PA) technique [11–16] and the temperature relaxation method (TRM) [17–21] respectively. These techniques have been shown by several authors to be simple reliable and non-destructive for measuring the thermal properties of different materials.

The PA technique looks directly at the heat generated in a sample due to nonradiative deexcitation processes, following the absorption of intensity modulated light. In the conventional experimental arrangement, a sample is enclosed in an airtight cell and exposed to a periodically chopped light beam. As a result of the periodic heating of the sample, the pressure in the cell oscillates at the chopping frequency and can be detected by a sensitive microphone coupled to the cell. The resulting signal depends not only on the amount of heat generated in the sample but also on how the heat diffuses through the sample. The quantity accounting for the rate of heat diffusion is the thermal diffusivity, α, which is related with the thermal conductivity (k), density (ρ) and specific heat capacity at constant pressure (c) through the expression:

$$k = \alpha \rho c \tag{1}$$

Beside the interest in their intrinsic value, the importance of the thermal diffusivity and thermal conductivity as physical quantities to be monitored is due to the fact that they are unique for each material as is the case of the optical-absorption coefficient.

The TRM, also known as temperature increment under constant illumination method [9] it is based in the fact that the relaxation of a closed system can be studied by perturbing an initial equilibrium state and monitoring the behavior in time of the variable of interest, such as the absolute temperature T. If the deviation from equilibrium is small enough, the temperature relaxation will follow the exponential law $T = T_0 \mathbf{e}^{-(t/\tau)}$, where t is the time, T_0 is the initial value of the temperature T, and τ is the relaxation time constant. In the case presented here, τ will depend on the specific heat capacity as will be evident in what follows.

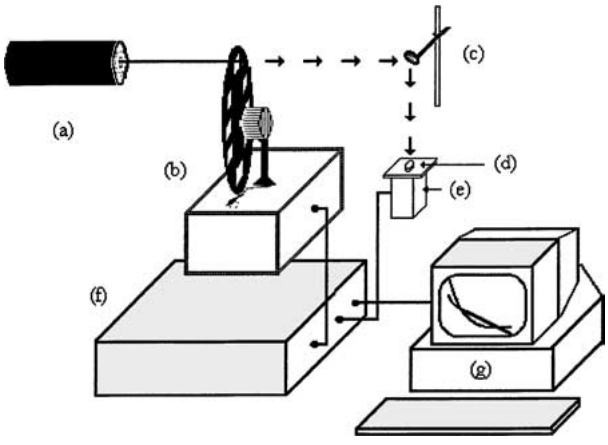

Figure 4 Experimental arrangement of the photoacoustic technique for thermal diffusivity measurement: (a) laser, (b) mechanical chopper (c) mirror, (d) sample, (e) photoacoustic cell, (f) lock-in amplifier, and (g) computer.

3.3.1. Thermal diffusivity. The photoacoustic (PA) technique

In our experimental setup for the PA technique, shown in Fig. 4, a 200 mW Ar^+ ion laser (Omnichrome 543-200MA) was used as a light source and its monochromatic light beam intensity was modulated at a frequency f by a Stanford Research Systems, Model SR-540, variable speed mechanical chopper before it normally impinged on the surface of the sample. The sample was placed in the cell (Fig. 5) and the PA chamber was connected to a sensitive acoustic detector (Bruel & Kjaer microphone). An interference filter was used to stop the UV plasma components of the laser. Part of the periodically incident light is converted into heat that propagates through the sample inducing pressure variations in the PA cell. The microphone converts the pressure variations into an electric voltage signal, the PA signal, which is detected by a lock-in amplifier Model SR-850 (Stanford Research Systems) interfaced to a personal computer through an IEEE-488 card. LabViEW 6.0 is used to record the data (amplitude of the PA signal) as a function of the modulation frequency. According to the thermal diffusion model for the photoacoustic effect for opaque solids, the PA signal amplitude as a function of the modulation frequency f is given by [15]:

$$A = C_0 \frac{1}{f\sqrt{\cos h(2\sqrt{f/f_c}) - \cos(2\sqrt{f/f_c})}} \tag{2a}$$

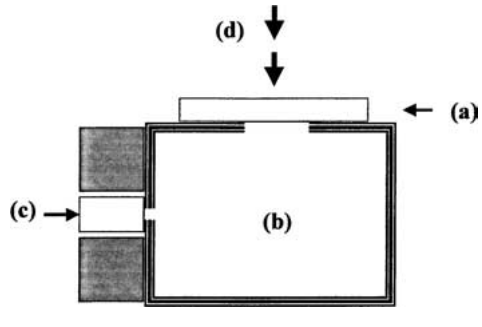

Figure 5 Scheme of the photoacoustic cell in a heat transmission configuration: (a) sample, (b) photoacoustic chamber, (c) detector, and (d) modulated light beam.

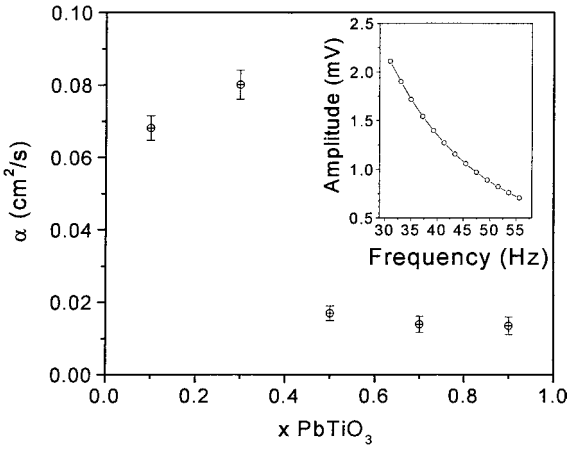

Figure 6 Thermal diffusivity vs. $PbTiO_3$ concentration in ceramic samples.

where,

$$C_0 = \frac{\sqrt{2\alpha_s\alpha_g}V_0I_0}{T_0l_gk_s\pi} \tag{2b}$$

Here α_s, l_s and k_s are, respectively, the thermal diffusivity, thickness and thermal conductivity of the sample. The subscript s denotes the sample (s) and gas (g) regions. T_0 is room temperature, I_0 is the incident beam intensity and V_0 is a quantity dependent on the microphone characteristics. The characteristic frequency $f_c = \alpha/\pi l_s^2$ represents the modulation frequency for which the thermal diffusion length ($\mu_s = \sqrt{\alpha/\pi f}$) is equal to the sample thickness l_s. The thermal diffusivity ($\alpha = f_c\pi l_s^2$) of the studied sample is obtained by fitting the experimental data of the PA amplitude signal as a function of f using Equation 2a, determining the f_c parameter and using the known value of the sample thickness l_s. The thermal diffusivity values obtained for the different $PbTiO_3$ concentrations are summarized in Fig. 6. The inset represents typical results of the PA measurements corresponding to an $x = 0.3$ sample. The solid line is the best fit to the experimental data using Equation 2a. The values of the thermal diffusivity change abruptly around $x = 0.4$–0.5 from the values for a pure phase of $SrTiO_3$ to those of pure $PbTiO_3$ in a reproducible manner.

3.3.2. Specific heat capacity. The temperature relaxation method

The specific heat capacity was measured using the temperature relaxation method (TRM) under continuous white light illumination. The experimental set up is shown in Fig. 7. The sample surfaces were sprayed with a very thin black paint film to improve light absorption. The samples were adiabatically suspended in an evacuated calorimeter with a pressure of about 10^{-3} mbar. Light was uniformly shined on one of the sample surfaces through an entrance glass window in the calorimeter. The temperature evolution of the back surface was monitored as a function of time using a programmable system interfaced to a personal computer.

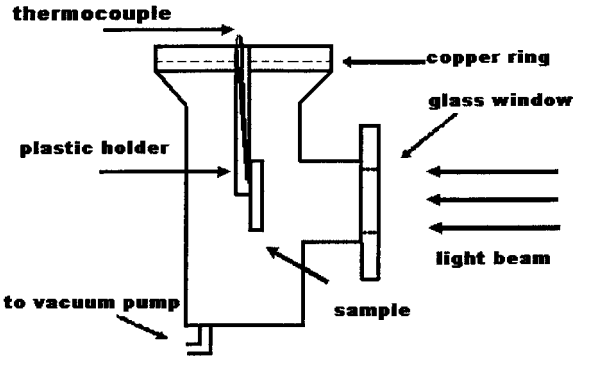

Figure 7 Experimental setup for measurements of the specific heat capacity.

The one-dimensional heat diffusion equation was used in the experiment. By solving this equation it can be shown that for times larger than the heat diffusion time $\cong l^2/\alpha$ of the sample the temperature rise is given by [9]:

$$\Delta T = \frac{I_0\alpha\tau}{l\kappa}(1 - e^{t/\tau}) \tag{3}$$

where I_0 is the intensity of the incident light beam, and

$$\tau = \frac{lC}{8\sigma\varepsilon T_0^3} \tag{4}$$

where σ is the Stefan-Boltzmann constant, C ($= \rho c$) is the heat capacity per unit volume, and T_0 is the ambient temperature. When the illumination is interrupted, the temperature decrease $\Delta T(t)$ is given by:

$$\Delta T(t) = \frac{I_0\alpha\tau}{lk}(e^{-t/\tau}) \tag{5}$$

The value of τ was obtained by fitting the experimental data to Equations 3 and 5. Fig. 8a shows a typical measurement performed in one of the samples by the TRM method, where the curves corresponding to increasing and decreasing temperatures are superimposed for visualization purposes. The solid curves represent the best fit to the corresponding data using Equations 3 and 5, taking τ as fitting parameter. From this value of τ the heat capacity per unit volume C was calculated using Equation 4 and these are shown in Fig. 8b. Table I is a summary of the measured thermal properties for each composition. By extrapolating the behavior of the specific heat with relative concentration to the cases of pure $PbTiO_3$ and $SrTiO_3$ it can be seen that the obtained values are smaller than those reported in the literature [22]. A small underestimation of the experimental values is expected due to perturbing factors such as the absorbing paint and this difference may be an indicative of the precision of the technique.

The thermal conductivity of the samples was calculated using the obtained values of the thermal diffusivity (α) and specific heat capacity (c) in Equation 1. The results of such calculation as a function of $PbTiO_3$ concentration are shown in Fig. 9. The thermal conductivity

TABLE I Thermal parameters for xPbTiO$_3$-$(1-x)$SrTiO$_3$ ceramics

Sample/thickness (μm)	Thermal diffusivity α(m^2/s)$\times 10^{-7}$	Density ρ(kg/m^3)$\times 10^3$	Specific heat capacity c (Jg^{-1}K^{-1})	Thermal conductivity k (Js^{-1}m^{-1}K^{-1})
$SrTiO_3$	35.8[a]	5.13[22]	$\approx$0.544[22]	$\approx$10
0.1/478 $\pm$ 7	68.07 $\pm$ 0.90	4.73	0.184 $\pm$ 0.01	5.92 $\pm$ 0.29
0.3/463 $\pm$ 10	80.31 $\pm$ 1.07	4.88	0.211 $\pm$ 0.01	8.27 $\pm$ 0.41
0.5/441 $\pm$ 7	17.38 $\pm$ 0.65	5.8	0.181 $\pm$ 0.01	1.825 $\pm$ 0.09
0.7/487 $\pm$ 8	13.92 $\pm$ 0.58	6.12	0.281 $\pm$ 0.01	2.39 $\pm$ 0.12
0.9/262 $\pm$ 2	13.49 $\pm$ 0.23	7	0.283 $\pm$ 0.01	2.67 $\pm$ 0.13
$PbTiO_3$	10.9[a]	7.96[22]	$\approx$0.462[22]	$\approx$4

[a]α for $PbTiO_3$ and $SrTiO_3$ were calculated using values from [22].

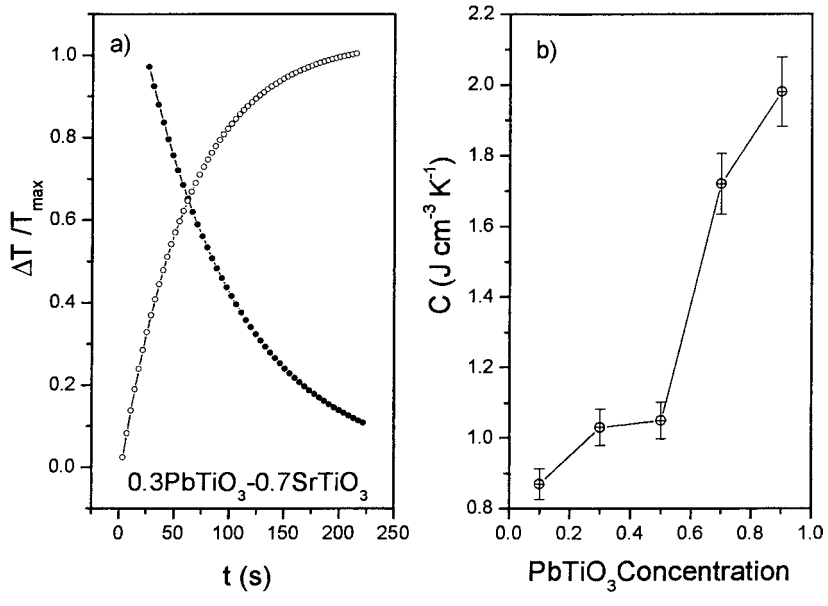

Figure 8 (a) Typical measurement performed in one of the samples by the thermal relaxation method. (b) Specific heat capacity as a function of $PbTiO_3$ concentration.

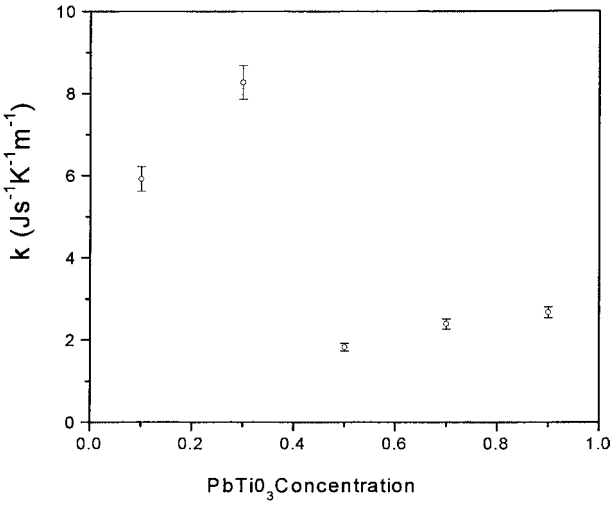

Figure 9 Thermal conductivity vs. $PbTiO_3$ concentration for the xPbTiO$_3$-$(1-x)$SrTiO$_3$ samples with $x = 0.1$, 0.3, 0.5, 0.7 and 0.9.

decreased with $PbTiO_3$ content after reaching a maximum value for $x = 0.3$ associated to the maximum in thermal diffusivity.

4. Conclusions

The electrical and thermal properties of the (x)PbTiO$_3$-$(1-x)$SrTiO$_3$ system with $x = 0.1$, 0.3, 0.5, 0.7 and 0.9 are discussed in this work. Electrical measurements reveal that once the system is formed with a specified mixture of the two materials, the polarization is almost linear with applied voltage for low $PbTiO_3$ content but develops a well defined ferroelectric behavior when this content increases. It is expected that when the $PbTiO_3$ content increases the relative abundance of the strained structure phase becomes more evident as shown by the thermoelectric analysis and the hysteretic behavior. The influence of one phase upon the other is particularly evident for $x = 0.5$ where a highly stressed structure is formed which manifests as a well defined transition at temperatures far from those of the extreme concentrations. For $x = 0.5$ the hysteresis loop is antiferroelectric-like. Such behavior is seen as a limit case of the strained structure leading to an antiparallel alignment of the ferroelectric domains. The usefulness of the temperature relaxation method and photoacoustic technique are demonstrated for the qualitative determination of the thermal properties of the xPbTiO$_3$ $(1-x)$SrTiO$_3$ system. Quantitatively, the thermal relaxation method seems to underestimate by a few percent the values of the specific heat. Nevertheless, such apparent shortcoming is not an intrinsic limitation of the method but a matter of taking all the influencing factors into account in the measurement.

Acknowledgments

This work was partially sponsored by CoNaCyT Proj. No. 33586-E and DGAPA-UNAM Proj. No. IN104000. We thank, V. García, P. Casillas, I. Gradilla, E. Aparicio, for their technical help.

References

1. GENE H. Heartling, *J. Amer. Ceram. Soc.* **82**(4) (1999) 797.
2. W. D. KINGERY, H. K.BOWEN and D. R. ULHMAN, "Introduction to Ceramics," 2nd ed. (A Wiley-Interscience Publication, John-Wiley & Sons, 1976) ingery; "Introduction to Ceramics" (Bowen, Uhlman, 1975) Chap. 12, p. 583.
3. W. ZHU, O. K. TAN, Q. YAN and J. T. OH, S*ens. Actuators* B **65** (2000) 366.
4. SCHOIRIO NOMURA and SHOZO SAWADA, *J. Phys. Soc. Japan* **10** (1955) 108.
5. B. DIBENEDETTO and C. J. CRONAN, *J. Amer. Ceram. Soc.* **51**(7) (1968) 365.
6. S. SUBRAHMANYAM and E. GOO, *Acta Mater.* **46**(3) (1998) 817.
7. Y. H. PAO, "Optoacoustic Spectroscopy and Detection" (Academic Press, NY, 1977).
8. MANDELIS and P. HESS, "Life and Earth Sciences" (SPIE Optical Engineering Press, Bellingham, Washington, third Volume of the Series: Progress in Photothermal and Photoacoustic Science and Technology, 1997).
9. A. M. MANSANARES, A. C. BENTO, H. VARGAS, N. F. LEITE and L. C. M. MIRANDA, *Phys. Rev.* B **42** (1990) 4477.
10. E. MARTÍNEZ, A. FUNDORA, O. BLANCO, S. GARCÍA, E. HEREDIA and J. M. SIQUERIROS, *Mat. Res. Soc. Symp. Proc.* **688** (2002) 265.
11. ROSENCWAIG and A. GERSHO, *J. Appl. Phys.* **47** (1975) 64.
12. M. YAÑEZ-LIMÓN, M. E. RODRIGUEZ, J. J. ALVARADO-GIL, O. ZELAYA-ANGEL, F. SANCHEZ SINENCIO, A. CRUZ-OREA, H. VARGAS, J. D. C. FIGUEROA, F. MARTINEZ-BUSTOS, J. L. MARTINEZ, J. GONZÁLEZ-HERNÁNDEZ and L. C. M. MIRANDA, *Analyst* **120** (1995) 1953.
13. D. P. ALMOND and P. M. PATEL, "Photothermal Science and Techniques in Physics and Its Applications" (Chapman and Hall, London, 1996) Vol. 10.
14. L. F. PERONDI and L. C. M. MIRANDA, *J. Appl. Phys.* **62** (1987) 2955.
15. A. CALDERÓN, R. A. MUÑOZ HERNÁNDEZ, S. A. TOMAS, A. CRUZ OREA and F. SÁNCHEZ SINENCIO, *ibid.* **84** (1998) 6327.
16. C. VÁZQUEZ LÓPEZ, A. CALDERÓN, M. E. RODRIGUEZ, E. VELASCO, S. CANO, R. COLAS and S. VALTIERRA, *J. Mater. Res.* **15** (2000) 85.
17. J. ALEXANDRE, F. SABOYA, B. C. MARQUES, M. L. P. RIBEIRO, C. SALLES, M. G. DA SILVA, M. S. STHEL, L. T. AULER and H. VARGAS, *The Analyst* **124** (1999) 1209.
18. E. MARÍN, P. DÍAZ, J. J. ALVARADO-GIL, J. G. MENDOZA-ALVAREZ, A. CRUZ-OREA, H. VARGAS and G. TORRES-DELGADO, *J. Phys. D: Appl. Phys.* **29**(4) (1996) 981.
19. RIECH, P. DÍAZ, T. PRUTSKIJ, J. MENDOZA, H. VARGAS and E. MARÍN, *J. Appl. Phys.* **86**(11) (1999) 6222.
20. RIECH, E. MARÍN, P. DÍAZ, J. J. ALVARADO-GIL, J. G. MENDOZA-ALVAREZ, H. VARGAS, A. CRUZ-OREA and M. VARGAS, *Phys. Stat. Sol.* (A) **169** (1998) 275.
21. E. MARÍN, H. VARGAS, P. DIAZ and I. RIECH, *ibid.* **179**(2) (2000) 387.
22. LANDOLT and BORNSTEIN, Numerical Data and Functional Relationships in Science and Technology, Ferroelectrics and Related Substances, (1981) p. 16.

Received 24 April
and accepted 7 October 2003